AGU PUBLICATIONS

Space Weather

RESEARCH ARTICLE
10.1002/2013SW001022

Key Points:
- Numerical model calculating radiation exposure in aviation
- Model validation with experimental data

Correspondence to:
D. Matthiä,
daniel.matthiae@dlr.de

Citation:
Matthiä, D., M. M. Meier, and G. Reitz (2014), Numerical calculation of the radiation exposure from galactic cosmic rays at aviation altitudes with the PANDOCA core model, *Space Weather*, *12*, doi:10.1002/2013SW001022.

Received 4 DEC 2013
Accepted 3 MAR 2014
Accepted article online 6 MAR 2013

Numerical calculation of the radiation exposure from galactic cosmic rays at aviation altitudes with the PANDOCA core model

Daniel Matthiä[1], Matthias M. Meier[1], and Günther Reitz[1]

[1]German Aerospace Center, Institute of Aerospace Medicine, Cologne, Germany

Abstract The increased radiation exposure at aviation altitudes is of public interest as well as of legal relevance in many countries. The dose rates that are elevated compared to sea level are mainly caused by galactic cosmic ray particles interacting with the atmosphere and producing a complex radiation field at aviation altitudes. The intensity and composition of this radiation field mainly depend on altitude, geomagnetic shielding, and primary particle intensity. In this work, we present a model based on Monte Carlo simulations, which retrospectively estimates secondary particle fluence as well as ambient dose equivalent rates and effective dose rates at any point in the atmosphere. This model will be used as the physical core in the Professional Aviation Dose Calculator (PANDOCA) software developed by the German Aerospace Center (Deutsches Zentrum für Luft- und Raumfahrt) for the calculation of route doses in aviation. The calculations are based on galactic cosmic ray spectra taking into account primary nuclei from hydrogen to iron by direct transport calculations of hydrogen and helium nuclei and approximating heavier nuclei by the number of protons equaling the corresponding atomic number. A comparison to experimental data recorded on several flights with a tissue equivalent proportional counter shows a very good agreement between model calculations and measurements.

1. Introduction

Life on Earth is, to a certain extent, protected from impinging cosmic ionizing radiation, i.e., the particles of solar and galactic origin by the Earth's magnetic field and its atmosphere [*Simpson*, 1983; *Reitz*, 1993; *European Radiation Dosimetry Group*, 2004]. Primary cosmic particles, which can reach the Earth's atmosphere, interact with its constituents and generate a secondary radiation field, the intensity of which reaches a maximum at an altitude of about 30 km and decreases underneath due to increasing atmospheric shielding. The maximum atmospheric shielding at sea level corresponds to a column mass of about 1000 g/cm^2, while the typical shielding provided by the atmosphere at aviation altitudes is on the order of 190 g/cm^2 to 350 g/cm^2 (about 39,000 ft to 27,000 ft). In addition to the atmospheric shielding, the Earth's magnetic field provides maximum protection from cosmic rays along the magnetic equator with a decreasing effect toward higher latitudes and negligible protection close to the magnetic poles.

The corresponding altitude and latitude dependent dose rates of the ambient dose equivalent and the effective dose increase from ground level to aviation altitudes and from low magnetic latitudes to high magnetic latitudes reaching values on the order of some 10 μSv/h at flight level (FL) 400 (40,000 ft) in the polar region during solar minimum when radiation exposure is at maximum within the solar cycle [*Meier et al.*, 2009]. Consequently, an aircrew spending several hundreds of hours in this natural radiation field each year is generally exposed to annual doses of more than 1 mSv, which is an internationally recommended threshold value for the implementation of radiation protection measures for workers who are occupationally exposed to ionizing radiation [*International Commission on Radiological Protection* (*ICRP*), 2007] and legally regulated in many countries, e.g., in the European Union. Radiation exposure to natural radiation sources as cosmic rays however was not regulated in the European Union until about two decades ago. In 1996, this gap of unequal treatment between employees being exposed to artificial and natural sources of radiation was closed by the European Union (EU) Council Directive 96/29/EURATOM. The purpose of this directive was to lay down basic safety standards for the protection of the health of workers and the general public against the dangers arising from ionizing radiation [*European Union* (*EU*), 1996]. In article 42 of the EU Council Directive, the assessment of the radiation exposure of aircrew is regulated. The assessment of exposure to natural radiation

sources can, in principle, be performed through measurement or model calculation. For operational purposes, calculation is generally applied in the airline industry [*Thierfeldt et al.*, 2009; *International Commission on Radiation Units and Measurements*, 2010]. This method requires a mathematical description of the calculation of dose rates in dependence on the flight route parameterized by a corresponding quantity of flight positions (longitude, latitude, and altitude) and solar activity as well as the time spent at each position. This information is usually given in the operational flight plan. Several models have been developed and operationally used for the assessment of the radiation exposure at aviation altitudes. The numerical model presented in this paper is based on a recently published model of the impinging particle spectrum [*Matthiä et al.*, 2013] and a Monte Carlo simulation of the particle transport in the atmosphere in contrast to the different approach of numerically solving the Boltzmann radiation transport equation [*Mertens et al.,* 2013]. Among other quantities, for example, secondary particle fluence or dose rates in silicon and water, the model is capable of calculating the effective dose rate and ambient dose equivalent rate and is used as the physical core in the software PANDOCA (Professional Aviation Dose Calculator) developed by the German Aerospace Center (Deutsches Zentrum für Luft- und Raumfahrt) and intended for the assessment of aircrew exposure. PANDOCA was part of an extensive intercomparison of numerical codes for the assessment of aircrew exposure [*Bottollier-Depois et al.*, 2012] which, apart from PANDOCA, includes most models available or under development at the time of the publication of the report: AVIDOS [*Latocha et al.*, 2009], CARI [*U.S. Federal Aviation Administration* (*FAA*), 2014], EPCARD [*Mares et al.*, 2009], FDOScalc [*Wissmann et al.*, 2010], IASON-FREE [*Felsberger et al.*, 2009], JISCARD-EX/PARMA [*Yasuda et al.*, 2008; *Sato et al.*, 2008], PCAIRE [*Lewis et al.*, 2004], PLANETOCOSMICS, QARM [*Lei et al.*, 2004], and SIEVERT [*Bottollier-Depois et al.*, 2007].

The model calculations are compared with in-flight measurements acquired by several radiation-measuring devices during the transition from solar cycle 23 to solar cycle 24, i.e., during solar minimum.

2. Material and Methods

The calculation of the radiation exposure at flight altitudes with the Monte Carlo approach requires several steps. The transport of primary galactic cosmic ray (GCR) particles through the magnetosphere and the atmosphere has to be calculated, and the resulting particle fluence at aviation altitude has to be converted to dose. In the following, the different parts of the procedure are described.

2.1. Galactic Cosmic Ray Model

The primary particle spectra described by the model of *Matthiä et al.* [2013] are used as input spectra for the calculation of the radiation exposure presented in this work. This model is based on the GCR International Organization for Standardization (ISO) standard, and the modulation of the GCR in the heliosphere is quantified by a single, empirical parameter, which is denoted by *W* and can be derived either from the measurements of the Advanced Composition Explorer (ACE) or count rates from any neutron monitor, e.g., Oulu or Kiel. In general, any detector measuring the GCR intensity could be used to calculate this parameter by establishing a relationship between the measured quantity and the model parameter *W*. It should be noted that *W* is not the Wolf number, which is used in the GCR ISO model, but directly derived from any measurement of the GCR intensity. During the periods of low-time lag between solar activity and GCR intensity, the numerical value of the parameter *W* is however similar to the Wolf number [cf. *Matthiä et al.*, 2013; *Nymmik et al.*, 1996].

Figure 1 shows the variation of the GCR intensity over the past 15 years as measured by the Kiel neutron monitor in Figure 1 (top) and the corresponding values of the *W* parameter below together with the International Sunspot Number (from http://sidc.oma.be/; Kiel data from http://www.nmdb.eu/). In addition to the linear conversion for the Oulu neutron monitor count rate given by *Matthiä et al.* [2013], we additionally provide here a rule for the Kiel neutron monitor count rates (*cr* = neutron monitor counts per minute):

$$W_{\mathrm{Kiel}} = -0.058 \cdot cr + 636.4. \quad (1)$$

This relationship was calculated by linearly fitting the *W* parameter derived from the ACE versus neutron monitor count rates averaged over one Bartel's rotation.

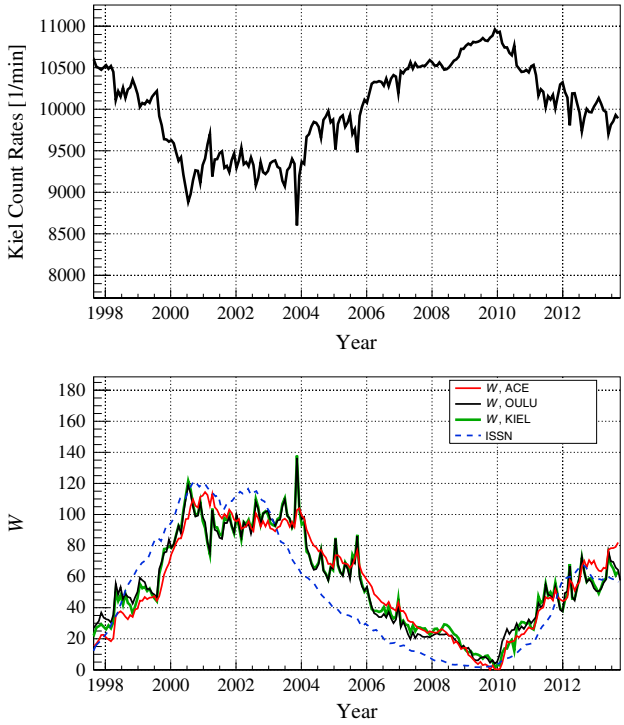

Figure 1. (top) Kiel neutron monitor count rates. (bottom) The *W* parameter quantifies the variation of the GCR intensity, where large values correspond to low intensity and vice versa. *W* can be derived from different detectors (e.g., Advanced Composition Explorer (ACE), red line; Oulu neutron monitor, black line; and Kiel neutron monitor, green line). The International Sunspot Number (ISSN) quantifies the solar activity.

It was shown in *Mrigakshi et al.* [2013] that there is little difference in the calculated radiation exposure in low Earth orbit for different sets for *W*, and the same is the case for the dose rates at aviation altitudes. The results presented in this paper are calculated using the Oulu neutron monitor count rates as input.

2.2. GEANT4 Transport Calculations

To calculate the transport of primary particles through the atmosphere, the Monte Carlo toolkit GEANT4 was used in version 9.4 patch 02 [*Agostinelli et al.*, 2003; http://geant4.cern.ch/]. The transport was calculated for primary proton and alpha particles in the energy range from 50 MeV to 1 TeV starting at an altitude of 180 km above ground, which means that more than 99.99% of atmospheric mass are below the starting location. The geometry and the model of the atmosphere are provided by PLANETOCOSMICS (http://cosray.unibe.ch/~laurent/planetocosmics/), which is a GEANT4 application. The atmospheric model implemented in PLANETOCOSMICS that was used for the simulations comprised 318 layers. The composition and pressure of the air contained in the layers were defined by the NRLMSISE-00 model [*Picone et al.*, 2002]. The physical lists describing the interactions of particles with matter and provided by GEANT4 that were used in the transport calculations were em_standard_opt3 for electromagnetic interactions, QGSP_BIC_HP for hadronic interactions, and JAM/JQMD for inelastic nucleus-nucleus interactions (for details see the GEANT4 "Physics Reference Manual"). The JAM/JQMD models are provided by an interface to an external FORTRAN code [*Koi et al.*, 2003].

The resulting particle fluence was registered at 40 different altitudes between sea-level and 100 km altitude with the majority lying below 20 km above ground. The following particles were considered for the calculation of the dose at a given altitude: protons, neutrons, photons, e^-, e^+, μ^-, μ^+, π^-, and π^+.

2.3. Magnetospheric Model

The well-known latitude dependence of the radiation exposure is related to the orientation and strength of the magnetic field of the Earth. The dipole-like form of the magnetic field of the Earth leads to a maximal attenuation of the galactic cosmic ray intensity close to the geomagnetic equator. The strength of this attenuation decreases with increasing geomagnetic latitude, and close to the magnetic poles, the galactic cosmic rays can reach the top of the atmosphere quasi unaffected by the Earth's magnetic field. The tilt and the shift of the magnetic field axis with respect to the rotation axis of the Earth lead to an asymmetric shielding effect.

The strength of the shielding effect can approximately be quantified by the position-dependent effective vertical cutoff rigidity R_C. The rigidity of a charged particle is defined as its momentum divided by its charge: $R = p/q$. In the following, the effective vertical cutoff rigidity will be referred to simply as cutoff rigidity. In the approach using the cutoff rigidity as a parameter for the magnetic shielding, it is assumed that at a given

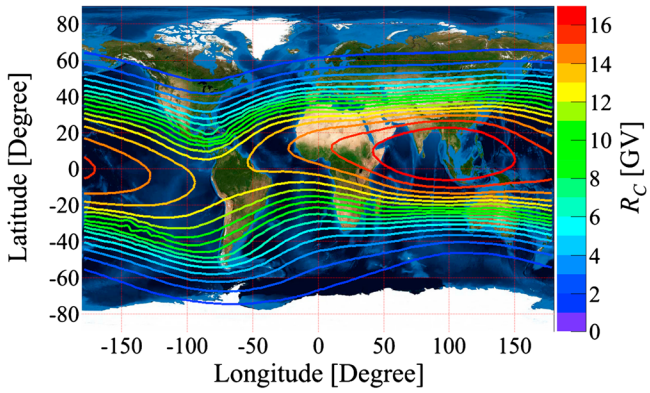

Figure 2. Effective vertical cutoff rigidity R_C calculated with PLANETOCOSMICS for 2005 using the International Geomagnetic Reference Field [*Maus et al.,* 2005]. The world map was provided by NASA (http://visibleearth.nasa.gov/).

location, no charged particle with rigidity below the cutoff rigidity traverses the magnetosphere and reaches the atmosphere, while all particles above the cutoff rigidity reach the location unaffected by the magnetic field of the Earth. If the cutoff rigidity is converted to kinetic energy, a lower threshold for the primary galactic cosmic ray spectrum can be defined. The cutoff rigidity is calculated from particles vertically arriving at the location of interest and lies in a rigidity interval, which is limited by the rigidity value below which no particle arrives at the location and the value above which all particles arrive at the given location (for details about cutoff rigidity terminology, see *Cooke et al.* [1991]).

The cutoff rigidities, which are used in the model presented in this work, were calculated with the GEANT4 application PLANETOCOSMICS using the International Geomagnetic Reference Field model for 2005 [*Maus et al.*, 2005]. The resulting cutoff rigidity world map is shown in Figure 2. The maximum of the cutoff rigidity is calculated for Southeast Asia. Accordingly, the lowest radiation exposure is expected in this region.

2.4. Calculation of Dose

Among other radiation parameters, the dose quantities relevant for radiation protection can be calculated by the model, i.e., the ambient dose equivalent $H^*(10)$ and the effective dose E as well as the corresponding dose rates. In a mixed radiation field of particles of type s (in this case secondary particles produced from interactions of GCR in the atmosphere), the ambient dose equivalent $H^*(10)$ can be calculated using energy-dependent fluence to dose conversion factors $c^s_{H^*(10)}(T)$, where T is the kinetic energy of the particle. If the energy spectrum of secondary particles is divided into energy intervals $\Delta T_j := [T_j - \Delta T_j/2, T_j + \Delta T_j/2]$, the dose can be approximated by the sum over the energy intervals and the secondary particle species:

$$H^*(10) \approx \sum_s \sum_j c^s_{H^*(10)}(T_j) \cdot F^s(\Delta T_j), \tag{2}$$

where $F^s(\Delta T_j)$ is the fluence, i.e., particles per area, of particle type s in the kinetic energy interval ΔT_j.Likewise, the effective dose E can be calculated as

$$E = \sum_s \sum_j c^s_E(T_j) \cdot F^s(\Delta T_j). \tag{3}$$

The factors $c^s_E(T)$ are fluence to dose conversion factors applicable to convert the particle fluence of particle type s to the corresponding contribution to the effective dose E.

The secondary particle fluence is calculated with the GEANT4 Monte Carlo toolkit in dependence on a primary particle type p and the primary particle's kinetic energy $\hat{T}$. Let $f^{p,s}_{\Delta\hat{T}_i}(\Delta T_j, d)$ be the fluence of a secondary particle type s in the energy interval ΔT_j at atmospheric depth d per fluence of the primary particle type p in the primary particle energy interval $\Delta\hat{T}_i$. The secondary particle fluence can then be calculated by summation over all primary particle types and energies and multiplication with the primary particle fluence $\hat{F}^p(\Delta\hat{T}_i)$ in the corresponding energy interval $\Delta\hat{T}_i$:

$$F^s(\Delta T_j, d) \approx \sum_p \sum_i \hat{F}^p(\Delta\hat{T}_i) \cdot f^{p,s}_{\Delta\hat{T}_i}(\Delta T_j, d). \tag{4}$$

Now if the radiation exposure at a certain depth is to be calculated, equation (4) has to be inserted in equation (2) for the ambient dose equivalent and in equation (3) for the effective dose. For the effective dose, for instance, that leads to

$$\begin{aligned} E &= \sum_s \sum_j c_E^s(T_j) \cdot \sum_p \sum_i \hat{F}^p(\Delta\hat{T}_i) \cdot f^{p,s}_{\Delta\hat{T}_i}(\Delta T_j, d) \\ &= \sum_p \sum_i \hat{F}^p(\Delta\hat{T}_i) \cdot g_E^p(\Delta\hat{T}_i, d), \end{aligned} \tag{5}$$

where $g_E^p(\Delta\hat{T}_i, d) \equiv \sum_s \sum_j c_E^s(T_j) \cdot f^{p,s}_{\Delta\hat{T}_i}(\Delta T_j, d)$ is a matrix, which is calculated from the secondary particle fluence per primary particle and the fluence to dose conversion factor for one of the dose quantities, in this case, the effective dose. The values of $g_E^p(\Delta\hat{T}_i, d)$ give the dose per primary particle fluence at a certain depth d and primary particle energy interval $\Delta\hat{T}_i$. If these matrices are known, the dose at arbitrary locations and times can be calculated by a simple summation and multiplication with the primary particle spectra. The values $f^{p,s}_{\Delta\hat{T}_i}(\Delta T_j, d)$ are precalculated with GEANT4 for a number of atmospheric depths. For altitudes lying between the precalculated values, the corresponding values of $g_E^p(\Delta\hat{T}_i, d)$ are calculated by linear interpolation.

For the ambient dose equivalent, the corresponding equation is

$$\begin{aligned} H^*(10) &= \sum_p \sum_i \hat{F}^p(\Delta\hat{T}_i) \cdot g^p_{H^*(10)}(\Delta\hat{T}_i, d) \\ g^p_{H^*(10)}(\Delta\hat{T}_i, d) &\equiv \sum_s \sum_j c^s_{H^*(10)}(T_j) \cdot f^{p,s}_{\Delta\hat{T}_i}(\Delta T_j, d). \end{aligned} \tag{6}$$

The modulation during the solar cycle is introduced through the time-dependent primary particle fluence $\hat{F}^p(\Delta\hat{T}_i)$, and the magnetic shielding is considered by restricting the sum over the primary particle energies to the values above the kinetic energy threshold $\Delta\hat{T}_i > \hat{T}_0$. The energy threshold at a given location is calculated from the cutoff rigidity:

$$\hat{T}_0 = \sqrt{(R_C \cdot q)^2 c^2 + m_0^2 c^4} - m_0 c^2, \tag{7}$$

where q is the charge of the primary particle, and m_0 is its rest mass; c is the speed of light.

If the primary particle fluence in equations (5) and (6) is replaced by the fluence rate, i.e., particles per area and time, the result is the corresponding dose rates. The fluence to dose conversion factors based on ICRP60 [*ICRP*, 1991] and summarized by *Pelliccioni* [2000] were used in this work. GCR nuclei from hydrogen to iron were considered as primary particles, but Monte Carlo simulations were performed for hydrogen and helium only. The contributions of all heavier nuclei were calculated by replacing the nucleus by a number of protons equaling the mass number of the primary ion and having the same energy per nucleon. The advantage of this approach is the drastically improved performance of the calculation. If the model is to be used for operational purposes, it is necessary to calculate the dose for thousands of flights, each containing hundreds of waypoints (for a 1 minute resolution of waypoints). Performing calculations for several coordinates showed that the contribution of heavier ions to the dose is below 10%, and the difference between the direct calculation of heavy ions and using the proton approach is less than a few percent.

It has to be emphasized that the method presented above is not restricted to the calculation of dose from primary GCR particles. Equations (5) and (6) can be applied to arbitrary input spectra, and especially for solar energetic particle events, the dose can be calculated using the same formalism and the same precalculated matrices, given that the primary particle spectrum is known. Additionally, if it becomes necessary in the future, it will be possible to use the more recent radiation weighting factors recommended in ICRP103 [*ICRP*, 2007] by including other fluence to dose conversion factors.

3. Results

The exemplary results of the model calculations are shown in Figure 3 for solar minimum conditions when the GCR intensity and the related radiation exposure reach their maximum. Figures 3a and 3b show the global ambient dose equivalent rate $dH^*(10)/dt$ at flight level 300 (FL300 = 30,000 ft = 9144 m) and flight level 400 (FL400 = 40,000 ft = 12,192 m), respectively. The coordinate range covers the whole globe from 90°N (+90°) to 90°S (−90°) and 180°W (−180°) to 180°E (+180°). Correspondingly, Figures 3c and 3d show the rate of the effective dose dE/dt. It is obvious that the lowest dose rate was calculated for the southeastern region

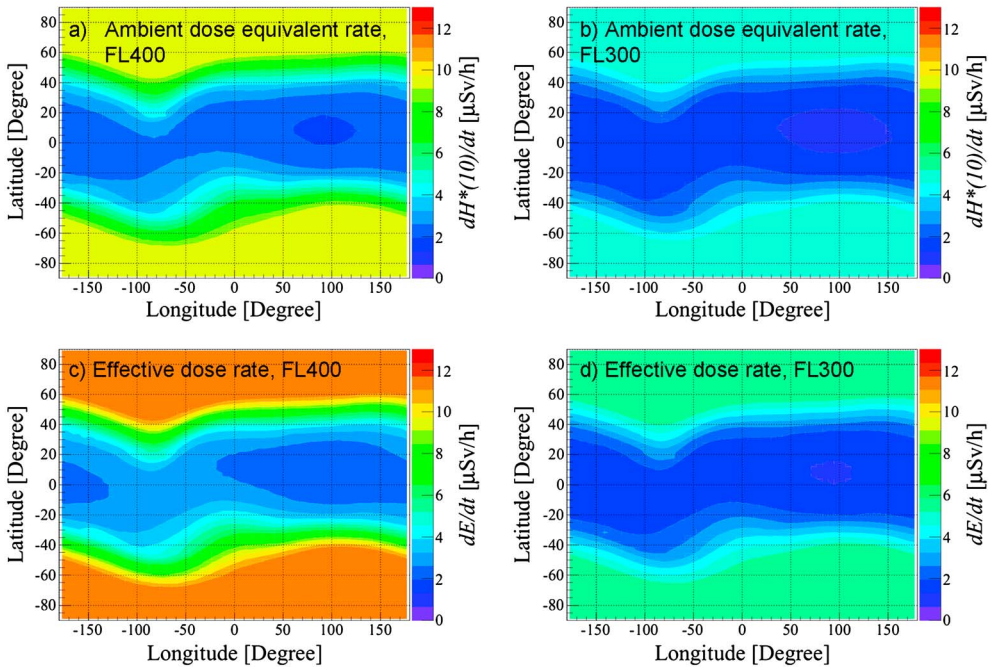

Figure 3. (a and b) Ambient dose equivalent rates and (c and d) effective dose rates calculated for flight level 400 (40,000 ft) and flight level 300 (30,000 ft) and solar minimum, i.e., GCR intensity maximum.

of Asia, where the geomagnetic shielding quantified by the cutoff rigidity reaches its maximum with $R_C \approx 17$ GV (Figure 1). Accordingly, the greatest dose rate is reached at high latitudes, where the geomagnetic shielding is minimal, and the cutoff rigidity is zero. It is also clearly visible that the dose rate at high latitudes decreases significantly to about 50% at lower flight altitudes (FL300) compared to the upper air space (FL400). Close to the equator at locations of great geomagnetic shielding, changing the flight level has a smaller effect on the dose rates, where the reduction is in the order of 35% to 40% for a change from FL400 to FL300. The reason for this behavior is the fact that two competing mechanisms reduce the radiation exposure: geomagnetic and atmospheric shielding. While the geomagnetic shielding is negligible at high latitudes and the atmospheric shielding is the dominant factor, the geomagnetic shielding becomes more important at low latitudes, and the relative shielding effect of the atmosphere is reduced.

The altitude dependence of the effective dose rate and the ambient dose equivalent rate during GCR maximum conditions, i.e., solar activity minimum, are shown in Figure 4. Additionally, the estimated contributions of the different secondary particle species are illustrated. Figures 4a and 4b show the effective dose rate (Figure 4a) and the relative contribution (Figure 4b) of the different particle species. Figures 4c and 4d illustrate the same for the ambient dose equivalent rate. The dose rates are increasing monotonically with increasing altitudes ranging from $dE/dt = 0.07$ μSv/h ($dH^*(10)/dt = 0.07$ μSv/h) on ground to $dE/dt = 11.6$ μSv/h ($dH^*(10)/dt = 9.5$ μSv/h) at FL400 (≈12.2 km). The largest contribution to these dose rates close to the ground is from secondary muons and neutrons, while at aviation altitudes, between 8.5 km and 12 km, and at low cutoff rigidities, neutrons and protons together account for about 80% of the dose and electrons, positrons, photons, and muons between 5% and 10% each. At the high cutoff rigidity of $R_C = 17$ GV, on the other hand, the contribution of protons is reduced, and electrons, positrons, and photons contribute significantly more. The direct contribution of secondary pions to the effective dose rate and the ambient dose equivalent rate was calculated to be below 0.5% and is not shown in Figure 4.

Besides the altitude dependency and the magnetic shielding, the intensity variation of galactic cosmic rays related to the solar cycle is the third major factor influencing the radiation exposure from GCR. Figure 5 illustrates this intensity variation reflected by the count rates of the ground-based neutron monitor station Oulu (Figure 5, top) and the related calculated dose rates (effective dose rate in Figure 5 (middle) and ambient dose equivalent rate in Figure 5 (bottom)) since 1970 at two altitudes, 40,000 ft (FL400) and 30,000 ft (FL300),

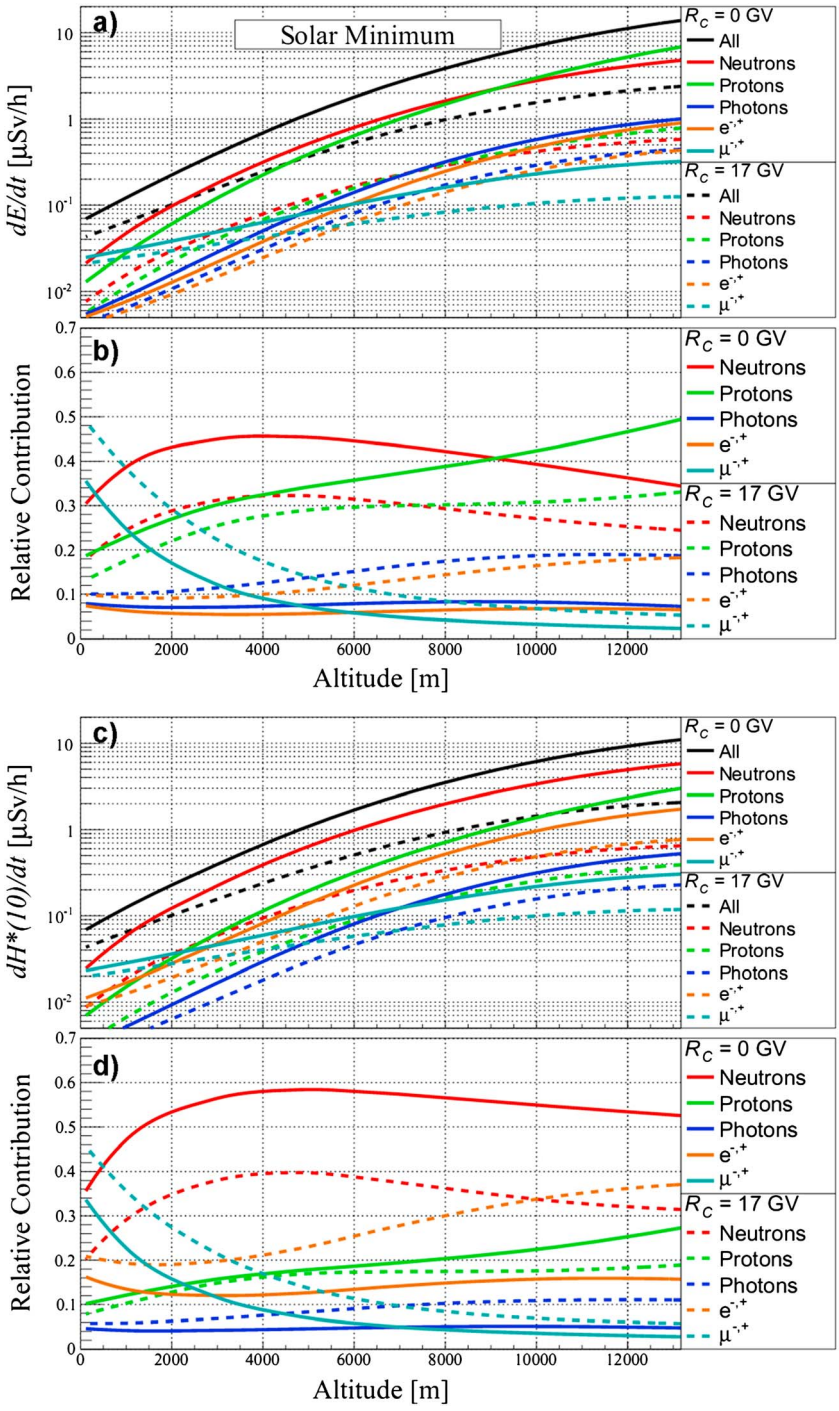

Figure 4. Altitude dependence of (a) the effective dose rate *dE/dt* and (c) the ambient dose equivalent rate *dH*(10)/dt* and the relative contribution of different (b and d) secondary particle species calculated for low geomagnetic shielding ($R_C = 0$ GV) and high geomagnetic shielding ($R_C = 17$ GV).

and two cutoff rigidities, $R_C = 0$ GV and $R_C = 17$ GV. At FL400, the effective dose rate varies between 5 μSv/h and 11.5 μSv/h (ambient dose equivalent rate: 4 μSv/h to 9.5 μSv/h) for low cutoff rigidity; for high cutoff rigidity $R_C = 17$ GV, the effective dose rate varies between 1.8 μSv/h and 2.2 μSv/h (ambient dose equivalent rate: 1.6 μSv/h to 1.9 μSv/h). At flight level 300, the calculated dose rates are significantly lower. Compared to the maximum in the dose rates reached in late 2009 (solar minimum), the values are reduced by several tens

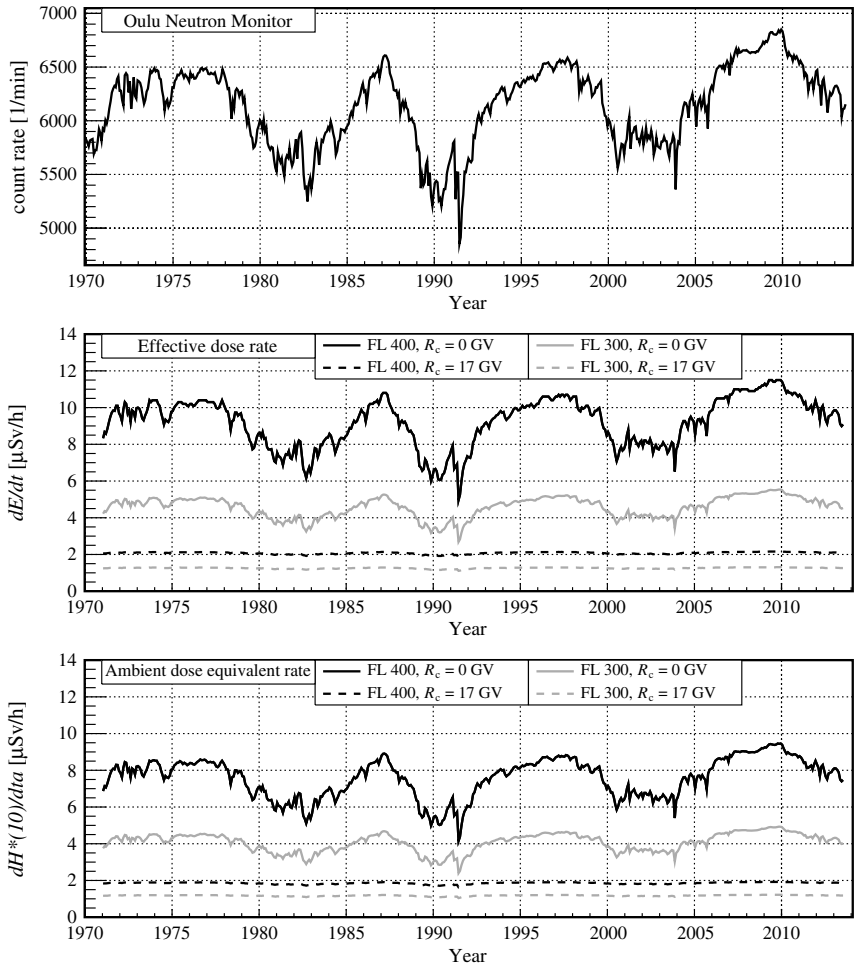

Figure 5. Solar cycle dependence of (top) the cosmic ray intensity on ground quantified by the Oulu neutron monitor station count rates and (middle) the corresponding calculated effective dose rate *dE/dt* and (bottom) ambient dose equivalent rate *dH**(10)*/dt*. The dose rates are calculated for low and high geomagnetic shielding (R_c = 0 GV, solid lines and R_c = 17 GV, dashed lines) at two altitudes (FL400, black lines and FL300, gray lines).

of percent during solar maximum conditions for flight level 400. At flight level 300, the relative variation is much smaller and mostly below 10%.

4. Comparison to Experimental Data

In 2006–2008, during the transition between solar cycle 23 and solar cycle 24, when the intensity of the radiation field at aviation altitudes was close to maximum, the German Aerospace Center performed measuring flights in cooperation with several German airline partners for the investigation of the corresponding radiation exposure. For this purpose, the ambient dose equivalent rate *dH**(10)*/dt* was measured with a HAWK2 instrument in dependence on the geomagnetic and atmospheric shielding [*Meier et al.*, 2009]. The HAWK2 is a tissue equivalent proportional counter (TEPC), which emulates a human cell with a diameter of 2 µm in order to measure the microdosimetric energy deposition therein. It was calibrated at the Pacific Northwest National Laboratory with sources that had been traced back to the corresponding standards of the National Institute of Standards and Technology [T. *Conroy*, 2004, also Unit Specific Test Documents, private communications, 2005, 2006, 2007].

The measuring flights were performed during stable solar conditions, i.e., the differences in the count rates of the Oulu neutron monitor, which is regarded as an indicator for the variation of the solar activity, were less than 4% [*Usoskin et al.*, 2001; http://cosmicrays.oulu.fi]. Furthermore, the *Kp* index was generally ≤3 during the

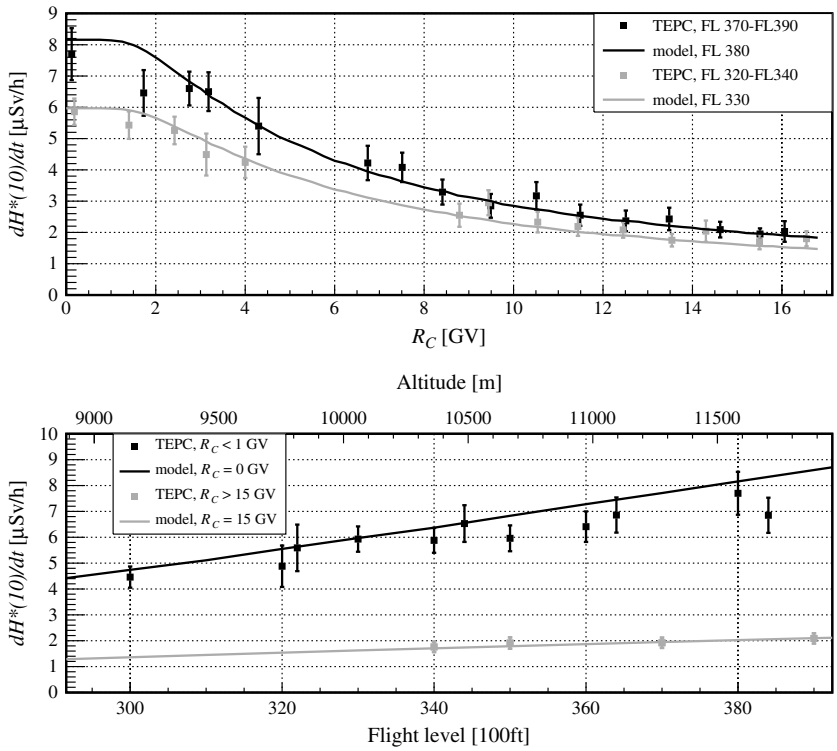

Figure 6. Results of the numerical model in comparison to ambient dose equivalent rates measured on several flights in 2007 and 2008 with a HAWK2 tissue equivalent proportional counter. Dose rate dependence on (top) the magnetic shielding (R_C) and on (bottom) the flight altitude. Numerical values are given in Table 1.

measuring flights, which is evidence for geomagnetically quiet conditions. Thus, the measured data could be pooled for all flights during this period in order to investigate the dependence of the radiation exposure on the atmospheric shielding parameterized by the flight altitude and the geomagnetic shielding parameterized by the effective vertical cutoff rigidity R_C.

The comparison of the PANDOCA core model calculations for the dependence of the ambient dose equivalent rate $dH^*(10)/dt$ on the flight level with measuring data is shown in Figure 6 (bottom) for the areas of weakest and strongest geomagnetic shielding, i.e., the polar and the equatorial regions. It can be stated that the model calculations agree well with the measuring data, although the calculations seem to slightly overestimate the measurements in the polar region at higher altitudes.

In Figure 6 (top), the comparison of the PANDOCA core model calculations for the dependence of the ambient dose equivalent rate $dH^*(10)/dt$ on the effective cutoff rigidity R_C is shown for the lower and the upper airspace. For this purpose, the measuring data were pooled from FL320 to FL340 for the lower airspace and from FL370 to FL390 for the upper airspace and compared with model calculations for the median flight level of FL330 and FL380, respectively. The effect of the geomagnetic shielding on the dose rate is demonstrated by the model, and the calculated values show a very good agreement with the measuring data within the statistical limits as well. To quantify the differences, the relative deviation Δ_i of the measured dose rate d_i^{meas} from the calculated dose rate d_i^{calc} for each point i in Figure 6 was calculated

$$\Delta_i = \left| \left(d_i^{\text{meas}} - d_i^{\text{calc}} \right) \right| / d_i^{\text{calc}} \tag{8}$$

The measured and calculated values for the two altitude and the two geomagnetic cutoff regions are given in Table 1, together with the relative deviation at each point.

Using the error of the measurements, it is possible to calculate the error of the relative deviations, and for each of the four sets of the data, the weighted mean of the relative deviation $\overline{\Delta}$ was derived: 0.05 (FL370–FL390), 0.06 (FL320–FL340), 0.08 ($R_C < 1$ GV), and 0.03 ($R_C > 15$ GV). Thus, all four groups show a mean relative deviation between 8 and 3% with the lowest in the $R_C > 15$ GV region.

Table 1. Values of the Ambient Dose Equivalent Rate *dH**(10)*/dt* Measured With the TEPC and Calculated With the PANDOCA and the Respective Relative Deviation (Equation (8)) for the Different Altitude and Cutoff Regions (cf. Figure 6)

Altitude Range: FL370–FL390																
R_C (GV)	0.1	1.7	2.8	3.2	4.3	6.7	7.5	8.4	9.5	10.5	11.5	12.5	13.5	14.6	15.5	16.1
*dH**(10)*/dt* (μSv/h)																
TEPC	7.7	6.5	6.6	6.5	5.4	4.2	4.1	3.3	2.9	3.2	2.6	2.4	2.4	2.1	2.0	2.0
TEPC error	0.8	0.7	0.5	0.6	0.9	0.6	0.5	0.4	0.4	0.4	0.3	0.3	0.4	0.3	0.2	0.3
PANDOCA	8.2	7.8	6.8	6.4	5.4	3.9	3.6	3.3	3.0	2.7	2.5	2.4	2.2	2.1	2.0	1.9
Relative deviation	0.06	0.18	0.03	0.02	0.00	0.07	0.13	0.01	0.05	0.16	0.01	0.00	0.10	0.01	0.00	0.07
Altitude Range: FL320–FL340																
R_C (GV)	0.2	1.4	2.4	3.1	4.0	8.8	9.4	10.5	11.4	12.5	13.5	14.3	15.5	16.6		
*dH**(10)*/dt* (μSv/h)																
TEPC	5.9	5.4	5.3	4.5	4.2	2.6	3.0	2.3	2.2	2.1	1.8	2.0	1.7	1.8		
TEPC error	0.4	0.4	0.4	0.7	0.5	0.4	0.4	0.3	0.3	0.3	0.2	0.3	0.2	0.2		
PANDOCA	6.0	5.9	5.4	4.9	4.4	2.5	2.4	2.2	2.0	1.9	1.8	1.7	1.6	1.5		
Relative deviation	0.02	0.08	0.02	0.08	0.03	0.01	0.23	0.07	0.09	0.09	0.01	0.21	0.08	0.20		
Cutoff Range: $R_C < 1$ GV																
Flight level	300	320	322	330	340	344	350	360	364	380	384					
dH(10)/dt* (μSv/h)																
TEPC	4.5	4.9	5.6	5.9	5.9	6.5	6.0	6.4	6.9	7.7	6.9					
TEPC error	0.4	0.8	0.9	0.5	0.5	0.7	0.5	0.6	0.7	0.8	0.7					
PANDOCA	4.7	5.6	5.6	6.0	6.4	6.6	6.8	7.3	7.5	8.2	8.3					
Relative deviation	0.06	0.12	0.01	0.01	0.08	0.00	0.13	0.12	0.08	0.06	0.18					
Cutoff Range: $R_C > 15$ GV																
Flight level	340	350	370	390	408											
dH(10)/dt* (μSv/h)																
TEPC	1.8	1.9	1.9	2.1	2.3											
TEPC error	0.2	0.2	0.2	0.2	0.3											
PANDOCA	1.7	1.8	2.0	2.1	2.2											
Relative deviation	0.03	0.07	0.02	0.00	0.05											

5. Summary

We present a numerical model, which calculates particle fluence, effective dose rates, and ambient dose equivalent rates caused by primary galactic cosmic rays at arbitrary locations in the atmosphere. The model uses Monte Carlo transport simulations to determine the secondary particle fluence in the atmosphere from galactic cosmic ray particles at any altitude in the atmosphere taking into account the geomagnetic shielding and the solar modulation. By using fluence-to-dose conversion factors, the dose rates are calculated. By replacing the conversion factors for the effective dose and ambient dose equivalent with conversion factors for dose in water, tissue, or silicon, the model also provides the capability to make direct comparisons to experimental data. Likewise, a future incorporation of conversion factors weighting the different particle contributions according to ICRP103 [*ICRP*, 2007] is possible. The comparison of the model results with measurements reveals an agreement within a few percent of the ambient dose equivalent rate.

Acknowledgments

The authors would like to thank M. Hubiak, N. Santen, and M. Wirtz for their support in performing the measuring flights and the corresponding data analysis, the Sodankyla Geophysical Observatory and the website team (http://cosmicrays.oulu.fi) for providing the Oulu neutron monitor data, the Kiel neutron monitor team for providing the Kiel neutron monitor data and the ACE CRIS instrument team, and the ACE Science Center for providing the ACE data. We also acknowledge the NMDB database (www.nmdb.eu), founded under the European Union's FP7 (contract 213007) for providing data.

References

Agostinelli, S., et al. (2003), GEANT4 – a simulation toolkit, *Nucl. Instrum. Methods Phys. Res., Sect. A*, *506*, 250–303, doi:10.1016/S0168-9002(03)01368-8.

Bottollier-Depois, J. F., P. Blanchard, I. Clairand, P. Dessarps, N. Fuller, P. Lantos, D. Saint-Lô, and F. Trompier (2007), An operational approach for aircraft crew dosimetry: The SIEVERT system, *Radiat. Prot. Dosim.*, *125*, 421–424, doi:10.1093/rpd/ncl555.

Bottollier-Depois, J. F., P. Beck, M. Latocha, V. Mares, D. Matthiä, W. Rühm, and F. Wissmann (2012), *Comparison of Codes Assessing Radiation Exposure of Aircraft Crew due to Galactic Cosmic Radiation*, EURADOS Rep. 2012-03, EURADOS, Braunschweig.

Conroy, T. (2004), Environmental Radiation monitor with 5" Tissue Equivalent Proportional Counter (TEPC), HAWK Version 2, Operations and Repair Manual, FWT Far West Technology Inc., Goleta.

Cooke, D. J., J. E. Humble, M. A. Shea, D. F. Smart, N. Lund, I. L. Rasmussen, B. Byrnak, P. Goret, and N. Petrou (1991), On Cosmic-Ray Cut-Off Terminology, *Nuovo Cimento*, *14 C*(3), 213–234, doi:10.1007/BF02509357.

EU (1996), Council Directive 96/29/EURATOM, *Off. J. Eur. Communities, L 159*(29.6.96), 1–114.

EURADOS (2004), *Cosmic Radiation Exposure of Aircraft Crew*, European Radiation Dosimetry Group report, European Communities, Luxembourg.

Felsberger, E., K. O'Brien, and P. Kindl (2009), IASON-FREE: Theory and experimental comparison, *Radiat. Prot. Dosim.*, *136*(4), 267–273, doi:10.1093/rpd/ncp128.

ICRP (1991), 1990 Recommendations of the International Commission on Radiological Protection, ICRP Publication 60, *Ann. ICRP*, *21*(1-3), 1–161.

ICRP (2007), The 2007 Recommendations of the International Commission on Radiological Protection, ICRP Publication 103, *Ann. ICRP*, *37*(2-4), 1–332.

ICRU (2010), ICRU Report No. 84, Reference Data for the Validation of Doses from Cosmic-Radiation Exposure of Aircraft Crew, *J. ICRU*, *10*(2).

Koi, T., M. Asai, D. H. Wright, K. Niita, Y. Nara, K. Amako, and T. Sasako (2003), Interfacing the JQMD and JAM Nuclear Reaction Codes to Geant4, Computing in High Energy and Nuclear Physics, SLAC-PUB-9978, doi:10.2172/813352.

Latocha, M., P. Beck, and S. Rollet (2009), AVIDOS – a software package for European accredited aviation dosimetry, *Radiat. Prot. Dosim.*, *136*(4), 286–290, doi:10.1093/rpd/ncp126.

Lei, F., S. Clucas, C. Dyer, and P. Truscott (2004), An atmospheric radiation model based on response matrices generated by detailed Monte Carlo simulations of cosmic ray interactions, *IEEE Trans. Nucl. Sci.*, *51*(6), 3442–3451, doi:10.1109/TNS.2004.839131.

Lewis, B. J., M. Desormeaux, A. R. Green, L. G. I. Bennett, A. Butler, M. McCall, and J. C. Saez Vergara (2004), Assessment of aircrew radiation exposure by further measurements and model development, *Radiat. Prot. Dosim.*, *111*(2), 151–171, doi:10.1093/rpd/nch333.

Mares, V., T. Maczka, G. Leuthold, and W. Rühm (2009), Air crew dosimetry with a new version of EPCARD, *Radiat. Prot. Dosim.*, *136*(4), 262–266, doi:10.1093/rpd/ncp129.

Matthiä, D., T. Berger, A. I. Mrigakshi, and G. Reitz (2013), A ready-to-use galactic cosmic ray model, *Adv. Space Res.*, *51*, 329–338, doi:10.1016/j.asr.2012.09.022.

Maus, S., et al. (2005), The 10th-generation international geomagnetic reference field, *Geophys. J. Int.*, *161*, 561–565, doi:10.1029/2005EO160006.

Meier, M. M., M. Hubiak, D. Matthiä, M. Wirtz, and G. Reitz (2009), Dosimetry at aviation altitudes (2006–2008), *Radiat. Prot. Dosim.*, *136*(4), 251–255, doi:10.1093/rpd/ncp142.

Mertens, C. J., M. M. Meier, S. Brown, R. B. Norman, and X. Xu (2013), NAIRAS aircraft radiation model development, dose climatology, and initial validation, *Space Weather*, *11*, 603–635, doi:10.1002/swe.20100.

Mrigakshi, A. I., D. Matthiä, T. Berger, G. Reitz, and R. F. Wimmer-Schweingruber (2013), Estimation of Galactic Cosmic Ray exposure inside and outside the Earth's magnetosphere during the recent solar minimum between solar cycles 23 and 24, *Adv. Space Res.*, *52*(5), 979–987, doi:10.1016/j.asr.2013.05.007.

Nymmik, R. A., M. I. Panasyuk, and A. A. Suslov (1996), Galactic cosmic ray flux simulation and prediction, *Adv. Space Res.*, *17*(2), 19–30, doi:10.1016/0273-1177(95)00508-C.

Pelliccioni, M. (2000), Overview of fluence-to-effective dose and fluence-to-ambient dose equivalent conversion coefficients for high energy radiation calculated using the FLUKA code, *Radiat. Prot. Dosim.*, *88*(4), 279–297.

Picone, J. M., A. E. Hedin, and D. P. Drob (2002), NRLMSISE-00 empirical model of the atmosphere: Statistical comparisons and scientific issues, *J. Geophys. Res.*, *107*(A12), 1468, doi:10.1029/2002JA009430

Reitz, G. (1993), Radiation environment in the stratosphere, *Radiat. Prot. Dosim.*, *48*(1), 5–20.

Sato, T., H. Yasuda, K. Niita, A. Endo, and L. Sihver (2008), Development of PARMA: PHITS-based analytical radiation model in the atmosphere, *Radiat. Res.*, *170*, 244–259, doi:10.1667/RR1094.1.

Simpson, J. A. (1983), Elemental and isotopic composition of the galactic cosmic rays, *Annu. Rev. Nucl. Part. Sci.*, *33*, 323–381, doi:10.1146/annurev.ns.33.120183.001543.

Thierfeldt, S., C. Haider, P. Hans, M. Kaleve, and F. Neuenfeldt (2009), Evaluation of the implementation of radiation protection measures for aircrew in EU member states, *Radiat. Prot. Dosim.*, *136*(4), 324–328, doi:10.1093/rpd/ncp170.

U.S. FAA (2014), Federal Aviation Administration, Radiobiology Research Team. [Available at http://www.faa.gov/data_research/research/med_humanfacs/aeromedical/radiobiology/, accessed 3 Feb. 2014]

Usoskin, I. G., K. Mursula, J. Kangas, and B. Gvozdevsky (2001), On-line database of cosmic ray intensities, in *Proc. 20th Int. Cosmic Ray Conf.*, vol. 9, pp. 3842, Copernicus Gesellschaft, ICRC, Hamburg.

Wissmann, F., M. Reginatto, and T. Möller (2010), The ambient dose equivalent at flight altitudes: a fit to a large set of data using a Bayesian approach, *J. Radiol. Prot.*, *30*, 513–524, doi:10.1088/0952-4746/30/3/006.

Yasuda, H., T. Sato, and M. Terakado (2008), A personal use program for calculation of aviation route doses, Proc. of 12th International Congress of the International Radiation Protection Association. [Available at http://www.irpa12.org.ar/fullpapers/FP3037.pdf.]